Photocatalytic CO_2 Reduction with Highly Efficient Homogeneous Fe(II) Catalysts based on bis-(pyrazol)phenantroline

Jorge Ferreira Jr,[1] Gabriela Uez,[1] Arthur L. Schmidt,[1] Camila Ebersol,[1] Daniel Pietezak,[1] Robson S. Oliboni,[2] Angélica V. Moro,[1] Diogo S. Ludtke,[1] Adriana C. A. Casagrande,[1] Pedro Migowski,[1] Fabiano S. Rodembusch,[1] Osvaldo L. Casagrande Jr[1,*]

[1] *Laboratory of Molecular Catalysis, Instituto de Química, Universidade Federal do Rio Grande do Sul, Avenida Bento Gonçalves, 9500, 90501-970, Porto Alegre, RS (Brazil).*

[2] *Grupo de Catálise e Estudos Teóricos, Centro de Ciências Químicas, Farmacêuticas e de Alimentos – CCQFA, Universidade Federal de Pelotas, 96010-900, Pelotas, RS, (Brazil)*

Resumo/Abstract

RESUMO

Uma série de complexos de ferro(II) contendo ligantes bis(pirazolil)fenantrolina foi sintetizada e avaliada como fotocatalisadores homogêneos para a redução de CO_2 a CO sob irradiação de luz visível. Os complexos (**Fe1–Fe4**) apresentaram alta atividade catalítica na presença de $[Ru(bipy)_3]^{2+}$ como fotossensibilizador e BIH como doador sacrificial de elétrons, em soluções saturadas com CO_2 de MeCN/H_2O. Dentre eles, o complexo **Fe2**, contendo grupos metila doadores de elétrons, obteve o maior número de voltas catalíticas (TON = 1318) após 24 h, com seletividade de 84% para CO. A variação sistemática do tempo de reação, concentração do catalisador e teor de água revelou que o **Fe2** mantém excelente atividade e seletividade mesmo em baixas concentrações, alcançando TON de 23138 e seletividade para CO de até 94%. Os resultados evidenciam o potencial de complexos de ferro, abundantes e sustentáveis, como catalisadores eficientes e seletivos para a fotorredução de CO_2 em condições brandas.
Palavras-chave: Redução de CO_2, fotocatálise, complexo de ferro, ligantes nitrogenados tetradentados

ABSTRACT -

A series of iron(II) complexes featuring bis(pyrazolyl)phenantroline ligands were synthesized and evaluated as homogeneous photocatalysts for CO_2 reduction to CO under visible light. The complexes (**Fe1–Fe4**) exhibited high catalytic activity in the presence of $[Ru(bipy)_3]^{2+}$ and BIH as photosensitizer and sacrificial electron donor, respectively, in CO_2-saturated MeCN/H_2O solutions. Among them, **Fe2**, bearing electron-donating methyl groups, achieved the highest turnover number (TON = 1318) after 24 h with 84% selectivity to CO. Systematic variation of reaction time, catalyst loading, and water content revealed that **Fe2** maintains excellent activity and selectivity even at low concentrations, reaching a TON of 23138 and CO selectivity up to 94%. These results highlight the potential of earth-abundant iron-based complexes as efficient and selective catalysts for CO_2 photoreduction under mild conditions.
Keywords: CO_2 reduction, photocatalysis, iron complex, nitrogen tetradentate ligands

1. Introduction

The increasing concentration of atmospheric carbon dioxide (CO_2) resulting from the combustion of fossil fuels and industrial processes has become one of the most pressing environmental challenges of our time. CO_2, as the primary greenhouse gas, significantly contributes to global warming and climate change. Addressing this issue requires not only capturing and sequestering CO_2 but also developing sustainable methods to convert this abundant and inert gas into value-added products.(1-3) Various strategies for CO_2 capture have been explored, including chemical absorption, adsorption using solid materials, and membrane separation. While these methods are effective at removing CO_2 from industrial emissions, they do not necessarily solve the issue of its accumulation. In this context, the conversion of CO_2 into useful chemicals such as carbon monoxide (CO), formic acid, or methane has gained considerable attention.(4-5) Among these, the reduction of CO_2 to CO is particularly appealing, as CO serves as a valuable precursor in the chemical industry, particularly in Fischer-Tropsch processes (FTP) and the production of synthetic fuels.(6-7) Among the numerous approaches for utilization of carbon dioxide as C1-building block its photocatalytic reduction, using homogeneous catalysts, represents a promising approach due to their potential to harness solar energy, an

abundant and renewable resource.(8-10) Homogeneous photocatalysts, in particular, have shown great potential in facilitating the challenging CO_2 reduction reaction under mild conditions while minimizing side reactions. A wide variety of homogeneous catalysts have been investigated for the photocatalytic reduction of CO_2 to CO, with transition metals at the forefront of this research. Catalysts based on metals such as ruthenium, rhodium, and iridium have demonstrated high activity and selectivity. However, these metals are rare and expensive, limiting their practical applications on a larger scale. As a result, attention has shifted toward earth-abundant first-row metal, such as Fe,(11-12) Mn,(13-14) Co,(15-17) and Ni(18-19) catalysts, which offer both economic and environmental benefits. Particularly, iron(II) complexes supported by polydentate nitrogen ligands such as such as bipyridine, phenanthroline, or porphyrin derivatives, (20-23) have emerged as promising candidates for the photocatalytic reduction of CO_2 to CO. In this paper, we will disclose a new family of homogeneous iron(II) catalysts containing bis-(pyrazolyl)phenantroline nitrogen ligands for the photocatalytic reduction of CO_2 to CO.

2. Experimental

3.1 Materials

All solvents used in the synthesis of catalysts and photocatalytic reactions were dried over a MBraun SPS-800 solvent purification system. Other solvents were dried from the appropriate drying agents under argon before use. $Fe(BF_4)_2.6H_2O$ and $[Ru(bipy)_3]Cl_2$ were purchased from Sigma-Aldrich and used as received. BIH (1,3-dimethyl-2-phenyl-2,3-dihydro-1H-benzo[d]-imidazole) was prepared according to the reported procedure.(24) ^1H and ^{13}C NMR chemical shifts are reported in ppm vs. $SiMe_4$ and were determined by reference to the residual solvent peaks. Elemental analyses were performed by the Analytical Central Service of the Institute of Chemistry-UFRGS (Brazil) and are the average of two independent determinations. High-resolution mass spectrometry (HRMS) data were collected on a Micromass Waters® Q-Tof spectrometer. Quantitative gas chromatographic analysis from the gas evolved in the headspace were performed with an Agilent Technologies 7890A GC system equipped with a thermal conductivity detector. CO and H_2 production were quantitatively assessed using a Petrocol HD capillary column (methyl silicone, 100 m length, 0.25 mm i.d. and film thickness of 0.5 µm) (36 °C for 15 min, then heating at 5 °C·min−1 until 250 °C).

3.2 General Procedure for the bis(pyrazolyl)phenanthroline ligands

In a dry, sealed tube under an inert atmosphere, equipped with a magnetic stirring bar, the respective pyrazole (2 mmol, 2 equivalents) and 10 mL of dry 1,4-dioxane were added. Potassium tert-butoxide (2 mmol, 224.5 mg, 2 equivalents) was then added, and the mixture was stirred magnetically at room temperature for 20 minutes. After this period, 2,9-dibromo-1,10-phenanthroline (1 mmol, 338 mg, 1 equivalent) was added, and the reaction mixture was heated to reflux (110 °C) under continuous magnetic stirring for 20 hours. Upon completion of the reaction, the mixture was cooled to room temperature, diluted with water, and extracted with dichloromethane (3 x 25 mL). The organic phase was dried over anhydrous $MgSO_4$, and the solvent was removed under reduced pressure. The crude products were obtained as solids and purified through vacuum filtration using a pentane: dichloromethane (9:1) mixture for washing or by column chromatography, utilizing a hexane:ethyl acetate eluent mixture.

3.2.1 2,9 bis-(pyrazol-1-yl)-1,10-phenanthroline (**bpzphen**). White solid. M.P.: 245-247 °C. Yield: 81%, 51 mg. ^1H NMR (400 MHz, $CDCl_3$) δ 9.12 (dd, J = 2.6, 0.5 Hz, 2H), 8.44 (d, J = 8.7 Hz, 2H), 8.40 (d, J = 8.7 Hz, 2H), 7.88-7.86 (m, 2H), 7.80 (s, 2H), 6.63 (dd, J = 2.6, 1.7 Hz, 2H). ^{13}C NMR (100 MHz, $CDCl_3$) δ 150.3, 143.7, 142.5, 139.0, 127.7, 127.6, 125.3, 113.4, 108.3. HRMS (ESI+): exact mass calculated for $[M+H]^+$ ($C_{18}H_{13}N_6$) requires m/z 313.1202, found: m/z 313.1193. Anal. Calc. for $C_{18}H_{12}N_6$: C: 69.22, H: 3.87, N: 26.91. Found: C: 68.86, H: 3.73, N: 26.52

3.2.2 2,9 bis-(3,5-dimethyl-1H-pyrazol-1-yl)-1,10-phenanthroline (**bpz^{Me2}phen**). White solid. M.P.: 215-218 °C. Yield: 89%, 65 mg. ^1H NMR (400 MHz, $CDCl_3$) δ 8.33 (d, J = 8.7 Hz, 2H), 8.27 (d, J = 8.7 Hz, 2H), 7.78 (s, 2H), 6.08 (s, 2H), 2.98 (s, 6H), 2.35 (s, 6H). ^{13}C NMR (100 MHz, $CDCl_3$) δ 152.6, 150.4, 144.2, 142.2, 138.6, 127.4, 125.6, 117.2, 109.3, 14.8, 13.8. Anal. Calc. for $C_{22}H_{20}N_6$: C: 71.72, H: 5.47, N: 22.81. Found: C: 71.46, H: 5.33, N: 22.57. HRMS (ESI^+): exact mass calculated for $[M+H]^+$ ($C_{22}H_{21}N_6$) requires m/z 369.1828, found: m/z 369.1822.

3.2.3 2,9 bis-(3-diphenyl-1H-pyrazol-1-yl)-1,10-phenanthroline (**bpz^{Ph}phen**). White solid. M.P.: 203-205 °C. Yield: 67%, 63 mg. ^1H NMR (400 MHz, $CDCl_3$) δ 9.08 (d, J = 2.6 Hz, 2H), 8.47 (d, J = 8.7 Hz, 2H), 8.30 (d, J = 8.7 Hz, 2H), 8.04-7.97 (m, 4H), 7.70 (s, 2H), 7.51-7.45 (m, 4H), 7.42-7.36 (m, 2H), 6.91 (d, J = 2.6 Hz, 2H). 13C NMR (100 MHz, $CDCl_3$) δ 154.1, 150.3, 143.7, 139.0, 132.8, 128.9, 128.7, 128.4, 127.6, 126.0, 125.2, 113.5, 105.8. HRMS (ESI+): exact mass calculated for $[M+H]^+$ (C30H21N6) requires m/z 465.1828, found: m/z 465.1820. Anal. Calc. for $C_{30}H_{20}N_6$: C: 77.57, H: 4.34, N: 18.09. Found: C: 77.11, H: 4.08, N: 17.79.

3.2.4 2,9-bis(3-(trifluoromethyl)-1H-pyrazol-1-yl)-1,10-phenanthroline (**bpz^{CF3}phen**). White solid. M.P.: 286-288 °C. Yield: 91%, 82 mg. ^1H NMR (400 MHz, $CDCl_3$) δ 9.15-9.07 (m, 2H), 8.50-8.38 (m, 4H), 7.87 (s, 2H), 6.87-6.80 (m, 2H). ^{13}C NMR (100 MHz, $CDCl_3$) δ 149.7, 145.2 (q, J = 39.0 Hz), 143.7, 139.7, 129.1, 128.5, 126.1, 121.1 (q, J = 268.0 Hz), 113.9, 106.4 (q, J = 2.0 Hz). HRMS (ESI+): exact mass

calculated for $[M+H]^+$ ($C_{20}H_{11}F_6N_6$) requires m/z 449.0949, found: m/z 449.0944.

3.3 Synthesis of iron complexes

3.3.1 $[Fe(bpzphen)(H_2O)_2](BF_4)_2$ (**Fe1**). $Fe(BF_4)_2{\cdot}6H_2O$ (0.1080 g, 0.32 mmol) and bpzphen (0.1000 g, 0.32 mmol) in degassed acetonitrile (10 mL) was stirred under nitrogen under for 24 h at 25°C. The orange solid was filtered off, washed with diethyl ether (3 x 5mL) and dried under vacuum. Yield: 0.1045 g (66%). Anal. Calc. for $C_{18}H_{16}B_2F_8FeN_6O_2$: C: 37.42, H: 2.79, N: 14.54. Found: C: 37.73, H: 3.07, N: 13.91.

3.3.2 $[Fe(bpz^{Me2}phen)(H_2O)_2](BF_4)_2$ (**Fe2**). This complex was prepared as described above for **Fe1**, starting from $bpz^{Me2}phen$ (0.1000 g, 0.27 mmol) and $Fe(BF_4)_2{\cdot}6H_2O$ (0.09112 g, 0.27 mmol) in acetonitrile (10 mL) to give **Fe2** as an orange solid (0.1200 g, 70% yield). Anal. Calc. for $C_{22}H_{24}B_2F_8FeN_6O_2$: C: 41.68, H: 3.82, N: 13.26. Found: C: 41.89, H: 3.89, N: 12.82.

3.3.3 $[Fe(bpz^{Ph}phen)(H_2O)_2](BF_4)_2$ (**Fe3**). This complex was prepared as described above for **Fe1**, starting from $dpz^{Ph}phen$ (0.1000 g, 0.22 mmol) and $Fe(BF_4)_2{\cdot}6H_2O$ (0.07425 g, 0.25 mmol) in acetonitrile (10 mL) to give **Fe3** as an orange solid (0.1330 g, 72% yield). Anal. Calc. for $C_{30}H_{24}B_2F_8FeN_6O_2$: C: 49.36, H: 3.31, N: 11.51. Found: C: 49.02, H: 3.14, N: 11.07.

3.3.4 $[Fe(bpz^{CF3}phen)(H_2O)_2](BF_4)_2$ (**Fe4**). This complex was prepared as described above for **Fe1**, starting from $dpz^{CF3}phen$ (0.1000 g, 0.22 mmol) and $Fe(BF_4)_2{\cdot}6H_2O$ (0.07425 g, 0.25 mmol) in acetonitrile (10 mL) to give **Fe4** as a yellow solid (0.1330 g, 81% yield). Anal. Calc. for $C_{30}H_{24}B_2F_8FeN_6O_2$: C: 49.36, H: 3.31, N: 11.51. Found: C: 49.02, H: 3.14, N: 11.07.

3.3 Photocatalytic CO_2 reduction

Photocatalytic CO_2 reduction was performed in a quick-fit Pyrex test tube (volume = 12.0 mL) containing a solution of the catalyst (0.05 mM), $[Ru(bipy)_3]^{2+}$ (0.3 mM) and BIH (0.11 M) in a CO_2-saturated $MeCN/H_2O$ solution (4.0 mL), irradiation for 24 h at 308 K. The tube was sealed with a rubber septum and then purged with acetonitrile-saturated CO_2 for 10 min. The solution was then irradiated by LED lamp (blue light, λ = 460 nm).

3. Results and Discussion

3.1 Synthesis and Characterization of iron complexes

The target tetradentate bis(pyrazolyl)phenantroline ligands were readily synthesized via nucleophilic aromatic substitution (SNAr) reaction between 2,9-dibromo-1,10-phenanthroline and the corresponding pyrazole in presence of potassium tert-butoxide (KOtBu) and using dioxane as solvent. This class of ligands was characterized by ^1H and ^{13}C NMR spectroscopy and elemental analysis and HRMS. The reaction of bis-(pyrazolyl)phenantroline ligands with 1 equiv of $Fe(BF_4)_2{\cdot}6H_2O$ in CH_3CN at room temperature yielded the corresponding iron(II) complexes which were isolated in good to excellent yields (66–93%) (Scheme 1). These complexes were characterized by elemental analysis.

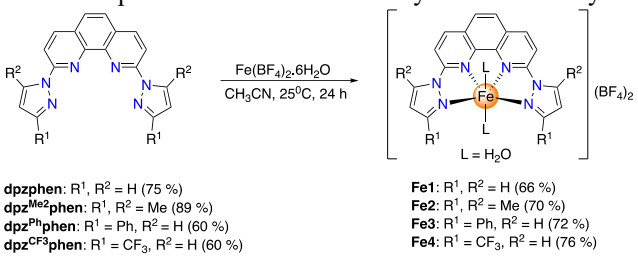

dpzphen: R^1, R^2 = H (75 %)
dpz^{Me2}phen: R^1, R^2 = Me (89 %)
dpz^{Ph}phen: R^1 = Ph, R^2 = H (60 %)
dpz^{CF3}phen: R^1 = CF_3, R^2 = H (60 %)

Fe1: R^1, R^2 = H (66 %)
Fe2: R^1, R^2 = Me (70 %)
Fe3: R^1 = Ph, R^2 = H (72 %)
Fe4: R^1 = CF_3, R^2 = H (76 %)

Scheme 1. Synthesis of iron(II) complexes

3.2 Light-driven CO_2 reduction

The catalytic performance of iron (**Fe1-Fe4**) complexes was evaluated under identical reaction conditions, including 50.0 μM catalyst, 0.3 mM $[Ru(bipy)_3]^{2+}$ as a photosensitizer, and 0.11 M BIH (1,3-dimethyl-2-phenyl-2,3-dihydro-1H-benzo[d]imidazole) as a sacrificial reductant in a CO_2-saturated $MeCN/H_2O$ solution at 308 K. The reactions were conducted under visible light irradiation (λ = 460 nm) for 24 hours, unless otherwise specified. The data is presented in Table 1. In the control experiment, conducted without any catalyst, just a small amount of CO (TON = 61) and H_2 (TON = 14) was produced (entry 1 in Table 1).

The iron complexes (**Fe1-Fe4**) exhibited high catalytic activity, with **Fe2** demonstrating the highest turnover number (TON) for CO production. Specifically, **Fe2** achieved a TON of 1318 after 24 hours as displayed in Figure 1.

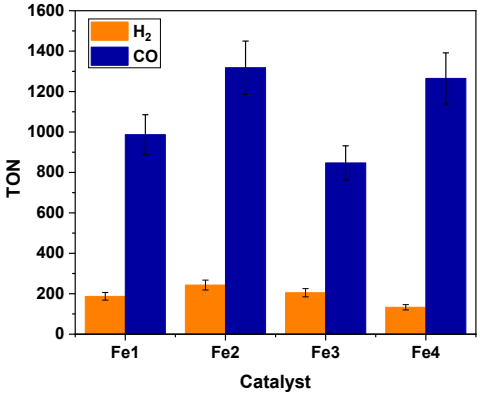

Figure 1. TON for photocatalytic CO_2-to-CO conversion by various iron catalysts in aqueous CH_3CN (7.5 % H_2O).

The superior catalytic performance of **Fe2** compared to the other iron complexes can be closely linked to the nature of the substituents on the 3- and 5-positions of the pyrazolyl ring in their ligand frameworks. Particularly, the electronic properties of the substituents at the 3- and 5-positions of the pyrazolyl ring can significantly alter the electron density at the metal center, influencing its redox behavior and ability to activate CO_2. e methyl) likely increases the electron

density on the metal center, favoring electron transfer to the CO_2. In **Fe2**, the electron-donating nature of the R-groups (i. Conversely, **Fe1** bearing naked pyrazolyl units and that one featuring feature electron-withdrawing groups (EWGs) (**Fe3**) exhibited lower TON values. However, **Fe4** bearing electron-withdrawing groups (CF_3) showed similar TON of 1265 and high selectivity towards production of CO (90.5%). Thus, the photocatalytic performance of iron complexes **Fe2** and **Fe4** reveals a compelling case of distinct electronic effects leading to similar CO production efficiency through different mechanistic pathways.

Table 1. Visible-light-drive catalytic reduction of CO_2 by iron complexes.[a]

Entry	Catalyst	Time (h)	H_2O (%)	TON (H_2)	TON (CO)	[H] (µmol)	[CO] (µmol)	Sel. CO (%)*	TOF (h^{-1})
1[b]	-	24	7.5	14	61	16.8	73.2	81	2.54
2	**Fe1**	24	7.5	187	987	37.4	197.4	84	41.1
3	**Fe2**	24	7.5	243	1318	48.6	263.6	84	54.9
4	**Fe3**	24	7.5	205	847	41.0	169.4	81	35.3
5	**Fe4**	24	7.5	133	1265	26.5	253.1	90.5	52.7
6	**Fe2**	4	7.5	51	311	10.2	62.2	86	77.7
7	**Fe2**	48	7.5	296	1578	59.2	315.6	84	32.9
8	**Fe2**	96	7.5	300	1593	60.0	318.6	84	16.6
9	**Fe2**	24	10	285	1352	57.0	270.4	82	56.3
10	**Fe2**	24	30	191	661	38.2	132.2	78	27.5
11[c]	**Fe2**	24	7.5	123	2086	12.3	208.6	94	86.9
12[d]	**Fe2**	24	7.5	276	4259	13.8	213.0	94	177.4
13[e]	**Fe2**	24	7.5	862	10168	20.7	263.9	93	423.7
14[f]	**Fe2**	24	7.5	2177	23138	27.2	289.2	91	964.1

a Reaction conditions unless specified otherwise: 50.0 mM catalyst, 0.3 mM $[Ru(bipy)_3]^{2+}$ and 0.11 M BIH, 24 h in a CO_2-saturated MeCN/H_2O solution (4 mL) at 308 K upon visible light irradiation (460 nm). b Without catalyst. c using catalyst concentration of 25.0 µM, [d] using catalyst concentration of 12.5 µM, [e] using catalyst concentration of 6.25 µM, [f] using catalyst concentration of 3.12 µM. All experiments were performed at least two times, having good reproducibility (error 5–10%).* SelCO = [mmol(CO)/(mmol(H_2)+mmol(CO)]x100.

Fe2, bearing electron-donating methyl groups at the 3- and 5-positions of the pyrazolyl ligands, exhibits the highest overall TON(CO) of 1318, driven by enhanced electron density at the iron center. This facilitates rapid CO_2 activation and reduction but also promotes undesired proton reduction, as reflected in its high TON_{H_2} of 243 and moderate CO selectivity (84%). In contrast, **Fe4**, functionalized with strongly electron-withdrawing CF_3 groups, displays a comparable TON_{CO} of 1265 despite a significantly lower TON_{H_2} of 133. The presence of CF_3 substituents likely stabilizes key catalytic intermediates and suppresses competitive hydrogen evolution, resulting in superior CO selectivity (90.5%). These observations suggest that while electron-donating groups accelerate CO_2 reduction, they also increase competition from HER, whereas electron-withdrawing groups, despite potentially retarding initial CO_2 activation, effectively direct the catalytic pathway toward CO formation with minimal side reactions. The comparable TON_{CO} values observed for **Fe2** and **Fe4** thus underscore a delicate trade-off between

reactivity and selectivity, highlighting the critical role of ligand electronic tuning in optimizing both efficiency and product distribution in CO_2 photoreduction catalysis.

To evaluate the impact of reaction conditions on the activity and CO/H_2 selectivity, a series of photocatalytic reactions were conducted using **Fe2**, varying the irradiation time, catalyst loading, and water content. The influence of irradiation time (4, 24, 48 and 96 h) on the catalytic was systematically investigated, as summarized in Table 1 (entries 4 and 6-8). The results reveal a strong correlation between the reaction time and the turnover numbers (TONs) for both H_2 and CO production, as well as the selectivity towards CO (Sel. CO) (Figure 2).

The turnover numbers (TONs) for both H_2 and CO production increased significantly with prolonged reaction times, demonstrating the catalyst's sustained activity. For instance, after 4 hours, the TONs were 51 for H_2 and 311 for CO, rising to 243 for H_2 and 1318 for CO after 24 hours. This upward trend continued up to 48 hours, with TONs reaching 296 for H_2 and 1578 for CO. However, beyond 48 hours, the TONs plateaued, with only marginal increases observed at 96 hours (300 for H_2 and 1593 for CO), suggesting that the system approaches a steady state, likely due to reactant depletion or the accumulation of inhibitory by-products. **Fe2** consistently showed a high selectivity for CO, around 84%, across all reaction times, preferring CO production over H_2.

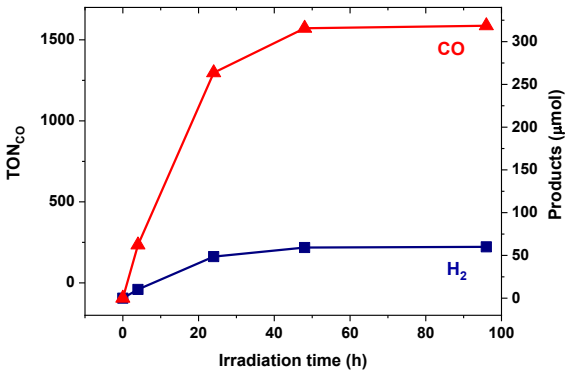

Figure 2. Evolution of the production of CO and H_2 with the irradiation time using **Fe2**.

The initial rapid increase in TONs during the first 24 hours indicates efficient catalytic activity under visible light irradiation, with the reaction kinetics slowing thereafter. This deceleration may be attributed to factors such as the gradual consumption of the sacrificial electron donor (BIH), the buildup of reaction intermediates, or potential catalyst deactivation. The near-constant TONs observed after 48 hours suggest a kinetic equilibrium, where the rate of CO_2 reduction is balanced by the rate of catalyst deactivation or reactant depletion.

The catalytic performance of **Fe2** was tested by varying the catalyst concentration from 3.12 to 50.0 μM, while keeping other reaction parameters constant. As presented in Fig 3, the TONs increase significantly as the concentration of the **Fe2** catalyst decreases in the reaction medium.

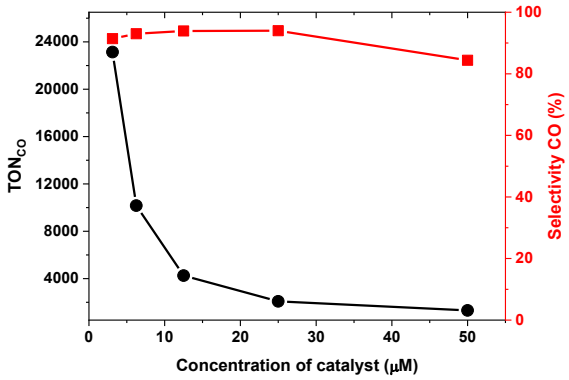

Figure 3. Concentration dependence of **Fe2** on TON_{CO} and selectivity.

For example, at the highest catalyst concentration of 50.0 μM, the TON_{CO} is 1318, while at the lowest concentration of 3.12 μM, the TON_{CO} reaches 10168. This inverse correlation between catalyst concentration and TON_{CO} can be attributed to several factors. First, at lower concentrations, each active site of the catalyst is more likely to be exposed to both CO_2 and light, enhancing the effective utilization of the catalyst. Higher concentrations, on the other hand, may lead to aggregation or overcrowding of catalyst molecules, which can hinder light penetration and reduce the availability of active sites. Second, the efficiency of electron transfer processes, critical for the photocatalytic reduction of CO_2, is improved at lower catalyst concentrations. Finally, mass transfer limitations become more pronounced at higher catalyst concentrations, particularly in a CO_2-saturated solution. Lower concentrations facilitate the diffusion of CO_2 to the active sites, thereby enhancing the overall reaction rate and TON. The selectivity for CO production remains consistently high across all catalyst concentrations, ranging from 84% to 94%. This high selectivity highlights the effectiveness of the **Fe2** catalyst in promoting CO_2 reduction over the competing hydrogen evolution reaction (HER). Notably, the selectivity for CO production shows a slight increase as the catalyst concentration decreases, reaching a maximum of 94% at 12.5 μM. This trend can be explained by the relative rates of CO_2 reduction and HER at different catalyst concentrations. At lower concentrations, the catalyst is more likely to be fully utilized for CO_2 reduction, as there are fewer active sites available for HER. Additionally, the reduced

likelihood of catalyst aggregation at lower concentrations may also contribute to the higher selectivity, as aggregated catalyst molecules may favor HER due to changes in the local electronic environment.

4. Conclusion

In this work, a series of iron(II) complexes supported by bis(pyrazolyl)phenanthroline ligands were synthesized and systematically investigated as homogeneous photocatalysts for the selective reduction of CO_2 to CO under visible light. Among the four complexes studied, **Fe2** exhibited the highest overall turnover number (TON_{CO} = 1318) and TOF (54.9 h^{-1}), attributed to the presence of electron-donating methyl groups that enhance electron density at the metal center, favoring efficient CO_2 activation. In contrast, **Fe4**, featuring electron-withdrawing CF_3 groups, achieved nearly the same TON_{CO} (1265) but with markedly higher selectivity for CO formation (90.5%) and significantly reduced hydrogen evolution ($TON(H_2)$ = 133), highlighting its superior ability to suppress side reactions. Complexes **Fe1** and **Fe3** showed intermediate performance, further supporting the conclusion that electronic modulation at the ligand periphery directly governs the balance between reactivity and selectivity. Extended reaction times and variations in catalyst concentration revealed that **Fe2** maintains high activity and selectivity under diluted conditions, reaching a TON_{CO} of 23138 and CO selectivity up to 94%. These findings suggest that optimized ligand frameworks can enhance light absorption, electron transfer, and CO_2 activation efficiency, even at low catalyst loadings. Complementary studies employing cyclic voltammetry and density functional theory (DFT) calculations are currently in progress to provide deeper insights into the mechanistic pathways involved.

5. Acknowledgments

The authors are gratefully acknowledged by RITE-FAPERGS (Grant/Award Number: 22/2551-0000386-9).

6. References

1. Nocera, D. G. Acc. Chem. Res. **2017**, *50*, 616−619.
2. Takeda, H.; Cometto, C.; Ishitani, O.; Robert, M. *ACS Catal.* **2017**, *7*, 70−88.
3. Pannwitz, A.; Klein, D. M.; Rodríguez-Jiménez, S.; Casadevall, C.; Song, H.; Reisner, E.; Hammarström, L.; Bonnet, S. *Chem. Soc. Rev*. **2021**, *50*, 4833−4855.
4. Appel, A. M.; Bercaw, J. E.; Bocarsly, A. B.; Dobbek, H.; DuBois, D. L.; Dupuis, M.; Fujita, E.; P. J. A.; Morris, R. H.; Peden, C. H. F.; Portis, A. R.; Ragsdale, S. W.; Rauchfuss, T. B.; Reek, J. N. H.; Seefeldt, L. C.; Thauer, R. K.; Waldrop, G. L. *Chem. Rev.* **2013**, *113*, 6621−6658.
5. Tang, B.; Xiao, F.-X. *ACS Catal.* **2022**, *12*, 9023− 9057.
6. Kunene, T.; Xiong, L.; Rosenthal, J. Proc. *Natl. Acad. Sci. U. S. A.* **2019**, *116*, 9693−9695.
7. Rosenthal, J. In Prog. Inorg. Chem., Karlin, K. D., Ed.; Wiley: Hoboken, NJ, **2014**, 59, 40.
8. Masdeu-Bultó, A. M.; Reguero, M.; Claver, C., *Eur. J. Inorg. Chem.* **2022**, e202100975.
9. Dalle, K. E.; Warnan, J.; Leung, J. J.; Reuillard, B.; Karmel, I. S.; Reisner, E. *Chem. Rev*. **2019**, *119*, 2752−2875.
10. Ma, F.; Luo, Z.-M.; Wang, J.-W.; Aramburu-Trŏselj, B. M.; Ouyang, G. *Coord. Chem. Rev.* **2024**, *500*, 215529.
11. Guo, Z.; Cheng, S.; Cometto, C.; Anxolabéhère-Mallart, E.; Ng, S.-M.; Ko, C.- C.; Liu, G.; Chen, L.; Robert, M.; Lau, T.-C., *J. Am. Chem. Soc.* **2016**, *138*, 9413− 9416.
12. Wang, Y.; Liu, T.; Chen, L.; Chao, D. *Inorg. Chem.* **2021**, *60*, 5590−5597.
13. Steinlechner, C.; Roesel, A. F.; Oberem, E.; Päpcke, A.; Rockstroh, N.; Gloaguen, F.; Lochbrunner, S.; Ludwig, R.; Spannenberg, A.; Junge, H.; Francke, R.; Beller, M. *ACS Catal.* **2019**, *9*, 2091−2100.
14. Bassan, E.; Inoue, R.; Fabry, D.; Calogero, F.; Potenti, S.; Gualandi, A.; Cozzi, P. G.; Kamogawa, K.; Ceroni, P.; Tamaki, Y.; Ishitani, O. *Sustain. Energy Fuels* **2023**, *7*, 3454−3463.
15. Zhang, X.; Yamauchi, K.; Sakai, K. *ACS Catal.* **2021**, *11*, 10436−10449.
16. Boudreaux, C. M.; Nugegoda, D.; Yao, W.; Le, N.; Frey, N. C.; Li, Q.; Qu, F.; Zeller, M.; Webster, C. E.; Delcamp, J. H.; Papish, E. T., ACS Catal. **2022**, *12*, 8718−8728.
17. Ho, P.-Y.; Cheng, S.-C.; Yu, F.; Yeung, Y.- Y.; Ni, W.-X.; Ko, C.-C.; Leung, C. F.; Lau, T.-C.; Robert, M. ACS Catal. **2023**, *13*, 5979−5985.
18. Hong, D.; Kawanishi, T.; Tsukakoshi, Y.; Kotani, H.; Ishizuka, T.; Kojima, T. *J. Am. Chem. Soc*. **2019**, 141, 20309−20317.
19. Manafe, S. Y.; Le, N.; Lambert, E. C.; Curiac, C.; Nugegoda, D.; Das, S.; Hunt, L. A.; Qu, F.; Whitt, L. M.; Fedin, I.;Hammer, N. I.; Webster, C. E.; Delcamp, J. H.; Papish, E. T. *ACS Catal.* **2024**, *14*, 6589−6602.
20. E. A. Mohamed, Z. N. Zahran and Y. Naruta, *Chem. Commun.,* **2015**, *51*, 16900.
21. S. Sinha and J. J. Warren, *Inorg. Chem.,* **2018**, *57*, 12650.
22. S. Fukuzumi, Y.-M. Lee, H. S. Ahn and W. Nam, Chem. Sci., **2018**, *9*, 6017.
23. A. Ogawa, K. Oohora, W. Gua and T. Hayashi, Chem. Commun., **2018**, *55*, 493.
24. Sampaio, R. N.; Grills, D. C.; Polyansky, D. E.; Szalda, D. J.; Fujita, E. *J. Am. Chem. Soc.* **2020**, *142*, 2413−2428.